Earth and Planetary Science Letters 414 (2015) 6–15

Contents lists available at ScienceDirect

Earth and Planetary Science Letters

www.elsevier.com/locate/epsl

Receiver function imaging of crustal suture, steep subduction, and mantle wedge in the eastern India–Tibet continental collision zone

Danian Shi [a,*], Zhenhan Wu [b], Simon L. Klemperer [c], Wenjin Zhao [b], Guangqi Xue [a], Heping Su [a]

[a] MLR Key Laboratory of Metallogeny and Mineral Assessment, Institute of Mineral Resources, CAGS, 26 Baiwanzhuang Road, Beijing 100037, China
[b] Chinese Academy of Geological Sciences, 26 Baiwanzhuang Road, Beijing 100037, China
[c] Department of Geophysics, Stanford University, Stanford, CA 94305-2215, USA

ARTICLE INFO

Article history:
Received 21 July 2014
Received in revised form 30 December 2014
Accepted 31 December 2014
Available online xxxx
Editor: P. Shearer

Keywords:
continental collision
crustal and upper-mantle structure
receiver-function imaging
Tibetan plateau
mantle suture
channel flow

ABSTRACT

To understand the along-strike variation of crustal deformation and tectonic processes in the India–Tibet continental collision zone, we deployed a linear array of broadband seismic stations along 92° E to image lithospheric structure. Our receiver-function cross-section reveals a prominent negative converter dipping ~20° north from ~10–55 km depth below sea-level, almost through the whole crust, beneath the southern Lhasa terrane. We interpret it to be a manifestation of the Yarlung–Zangbo suture zone (YZS) separating the continental crust of the Indian and Eurasian plates. This implies the hypothesized channel-flows of Indian middle crust extruding southwards from Tibet are limited at this longitude to the southernmost portion of the Lhasa terrane. A positive converter, consistent with previous suggestions of eclogite formation, is seen about 10–15 km above the Moho and continuing 50 km north of the 20°-dipping YZS converter. We image this positive converter continuously from ~60 km south of the surface trace of the YZS to the vicinity of the Jiali fault, supporting the interpretation of sub-horizontal underplating of Tibetan crust by Indian crust to ~31° N at 85° E on the Hi-CLIMB transect. However, we also show a negative mantle converter sub-parallel to the crustal YZS converter, from the northern limit of the underplating Indian lower crust to at least 140 km depth, that we interpret as the base of Tibetan lithosphere overlying an asthenospheric mantle wedge. Based on the lithospheric structure observed in this and other studies, we infer that Indian mantle lithosphere currently detaches from Indian lower crust at the "mantle suture" that is nearly 50 km south of the surface trace of the YZS at 92° E, south of the mantle suture suggested by INDEPTH transect beneath the surface trace of the YZS at ~90° E, and far south of the mantle suture suggested to be at the 31° N northern limit of underthrusting Indian lower crust suggested by Hi-CLIMB transect at ~85° E. A change from underplating in the west to steep subduction in the east can reconcile all these observations.

1. Introduction

The Tibetan Plateau is the spectacular consequence of the ongoing India–Eurasia continental collision beginning ~50 Myr ago (e.g., Argand, 1924; Molnar and Tapponnier, 1975; Yin and Harrison, 2000; Leech et al., 2005). Numerous seismic studies over the last three decades have studied the formation and evolution of the plateau. There is now widespread agreement that Indian lower crust is underthrust beneath the Himalaya (Zhao et al., 1993; Schulte-Pelkum et al., 2005) and has underplated beneath southern Tibet to ~31° N (Kind et al., 2002; Nábělek et al., 2009). Because of the great thickness of Tibetan crust, the preferred method of imaging Tibetan lithosphere has become receiver-function common-conversion point (CCP) images along linear transects, the best-known of which are INDEPTH at c. 90° E (e.g. Kind et al., 2002; Kosarev et al., 1999; Kumar et al., 2006; Shi et al., 2004; Zhao et al., 2011) and Hi-CLIMB at ~85° E (e.g. Nábělek et al., 2009; Wittlinger et al., 2009) (Fig. 1, inset). Even on INDEPTH and Hi-CLIMB, however, the Yarlung–Zangbo suture zone (YZS) that separates Indian and Asian continental crust has largely eluded imaging, and the plate geometry within the mantle has remained controversial.

The post-collisional convergence between the two continents is estimated to be at least 1000–1400 km, and about a quarter of the

* Corresponding author. Tel.: +86 10 68999061; fax: +86 10 68327263.
E-mail addresses: shidanian@cags.ac.cn (D. Shi), wuzhenhan@sohu.com (Z. Wu), sklemp@stanford.edu (S.L. Klemperer), zhaowj@cae.cn (W. Zhao), xueguangqi@cags.ac.cn (G. Xue), suheping1950@163.com (H. Su).

http://dx.doi.org/10.1016/j.epsl.2014.12.055
0012-821X/

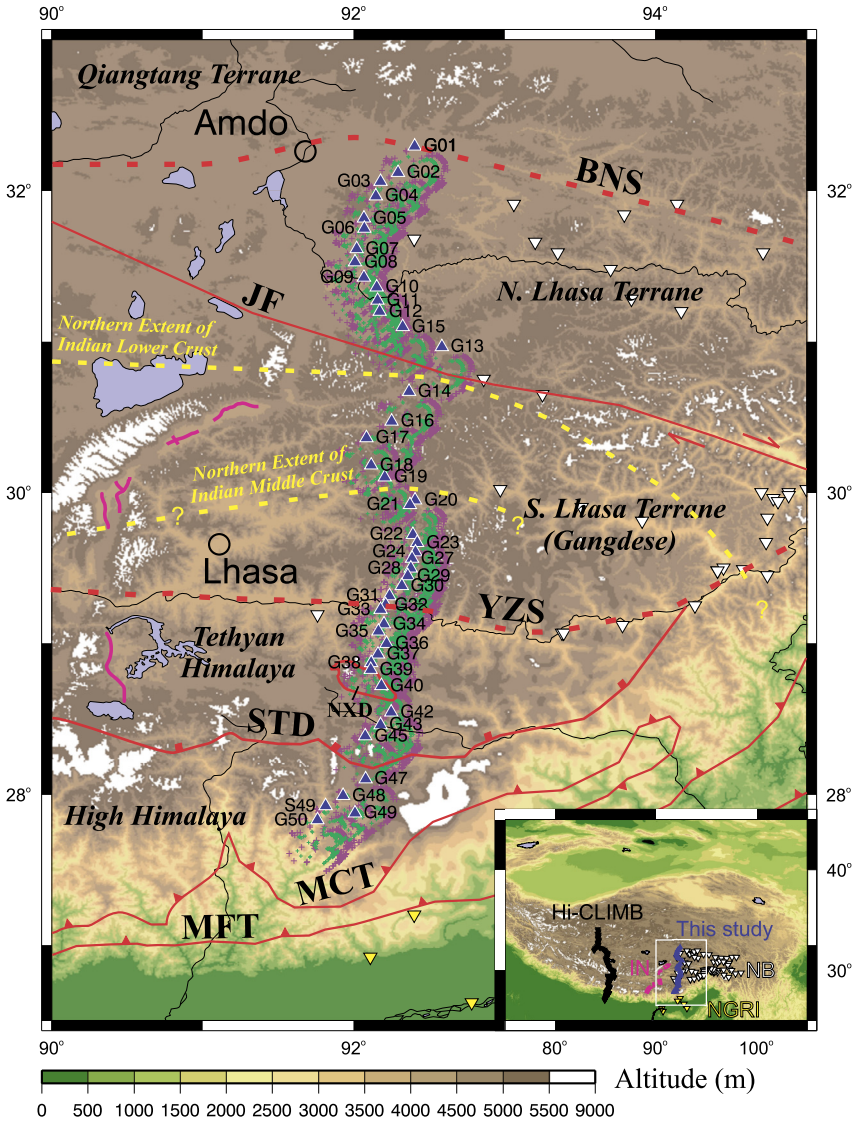

Fig. 1. Location of our broadband seismic stations (blue triangles) deployed across the India–Tibet collision zone. Dashed red lines mark the Yarlung Zangbo (YZS) and Bangong–Nujiang (BNS) sutures. Red lines delineate the Main Frontal Thrust (MFT), Main Central Thrust (MCT), South Tibet Detachment (STD), Nielaxiongbo dome (NXD) and the dextral Jiali fault (JF). Dashed yellow lines show the inferred northern limits of middle and lower Indian crust from observations of the doublet in this study and by Zurek (2008). Small green and purple crosses indicate all the piercing points of P-wave receiver functions at 45 and 65 km b.s.l., corresponding approximately to the positions of the top and bottom of Indian lower crust. Pink lines show INDEPTH reflection profiles. White triangles are seismic stations of the Namche Barwa experiment (Zurek, 2008). Yellow triangles are Indian stations used by Uma Devi et al. (2011). Inset shows the extent of this map (white rectangle), the Hi-CLIMB main-profile seismic stations (black), INDEPTH reflection profiles (pink, "IN"), the Namche Barwa seismic stations (white triangles, "NB") and National Geophysical Research Institute seismic stations (yellow triangles, "NGRI") on the topographic map of the Tibetan plateau.

convergence is believed to have been absorbed across the southern Tibetan plateau (>360 km across the Himalaya, and >60 km across the Gangdese thrust system) (Yin and Harrison, 2000). How this shortening has been accommodated is not well known and a variety of mechanisms have been proposed to explain the formation and tectonic evolution of the plateau. One class of models holds that the large and fairly uniform elevation of the plateau is achieved by diffuse deformation of Asian lithosphere (e.g. England and Houseman, 1989), that the outward growth of the plateau and the varying gradients of its margins are controlled by channel flow within a partly ductile lower crust (Clark and Royden, 2000; Beaumont et al., 2004), and that the superimposed east–west extension observed within the plateau is derived from subsequent delamination or convective removal of thickened mantle lithosphere (e.g. England and Houseman, 1989). Another class of models regards the Indian and Tibetan lithospheres as relatively rigid plates, with the convergence accommodated by partitioning into strike-slip and thrusting deformation due to the oblique configuration between the strike-slip faults and the northward subduction of the Indian plate (Dewey and Burke, 1973; Tapponnier et al., 2001). Numerical modeling shows Indian continental lithosphere is subductable if its upper crust is scraped off, so that Indian subduction is theoretically feasible (Capitanio et al., 2010). A third class of models suggests that cratonic Indian lithosphere is not subductable, and that Indian lithosphere may underthrust horizontally immediately beneath the crust of the overlying plate (Argand, 1924) after the break-off of the Indian oceanic slab at ~45 Ma (Powell and Conaghan, 1973). The interpreted receiver-function image of sub-horizontal underplating of Indian lower crust beneath southern Tibet (Nábělek et al., 2009) and the efficient propagation of Pn and Sn waves beneath the southern Tibetan plateau (Ni and Barazangi, 1983) are supporting evidence for the underplating model.

'Bright spots' with negative polarity on the INDEPTH seismic profiles in southern Tibet, shallower than 20 km depth, have been interpreted as an indication of widespread partial melt within the mid-crust (Nelson et al., 1996), and have provided strong support for the channel flow model (Beaumont et al., 2004). The INDEPTH profiles were carried out along the N-S trending grabens. Whether the results on the INDEPTH profiles can be generalized to the entire plateau is a major question: Hetényi et al. (2011) show that upper-crustal low-velocity zones imaged by the Hi-CLIMB array are small, discontinuous and localized under grabens, arguing against the existence of widespread partial melt within the Tibetan crust. Yang et al. (2012), however, use ambient noise tomography to resolve continuous low-velocity zones on a large scale in the mid-lower crust of the entire plateau. The depth and location of channel flow in Tibet remain uncertain.

Kosarev et al. (1999) show the Indian lithospheric mantle has detached from Indian crust beneath the surface trace of the YZS, and suggest the location of the "mantle suture" (the northern limit, at the Moho, of Indian lower lithosphere actively subducting deeper into the mantle) to be at ~29.5° N at ~90° E, supporting the subduction of the Indian plate. However, Nábělek et al. (2009) suggest the Indian lithospheric mantle remains attached to the sub-horizontal Indian lower crust to ~31° N, and interpret the mantle suture at ~31° N at ~85° E, favoring the underplating model. The large difference in interpreted northern extent of India is surprising because the trace of the YZS trends west–east at ~29.5° N between the INDEPTH and Hi-CLIMB seismic transects. It has remained uncertain whether one of these interpretations is wrong (in part because of the difficulty in imaging small impedance contrasts in the upper mantle), or if indeed there is substantial along-strike variation in the geometry of the orogen.

Most interpretations of the Himalayan and southern Tibet have been made assuming large-scale west–east uniformity of the orogen co-axial with the surface trace of the YZS. However, a growing body of both geophysical and geological work points to major west–east along-strike variations in subduction style. Some P-wave arrival time tomograms show sub-horizontal underthrusting of the Indian mantle lithosphere beneath the entire plateau in west Tibet, and subduction at moderate angle beneath the southern Lhasa terrane in central Tibet, but no northward extent of India beneath Tibet east of 92° E (Li et al., 2008). Gravity data indicate that the eastern Gangdese is characterized by negative isostatic residual gravity anomaly, in contrast to the positive anomaly in the central and western Gangdese (He et al., 2014). Geological observations indicate that post-collisional (8–24 Ma) ultrapotassic magmatism is most concentrated in central to western Gangdese (Zhao et al., 2009), but that intensive porphyry metallogenesis and adakitic magmatism (involving a juvenile mantle component) (12–18 Ma) mainly occurred in the central to eastern Gangdese (Hou and Cook, 2009). All these observations suggest a variation in mantle structure from west to east may exist beneath southern Tibet.

There is no doubt that the indentation of the Indian plate under southern Tibet has played a key role in the deformation and tectonic evolution of the plateau. A knowledge about how it varies along the collisional zone will allow us to achieve a better understanding of stress regime, crustal and upper mantle deformation, and magmatic and metallogenic processes in the southern plateau. For this purpose, we carried out a passive-source seismic experiment at ~92° E in southeastern Tibet. In this study we present our receiver-function results about the crustal and upper-mantle structure of the eastern India–Tibet collision zone.

2. Data and method

Our "Gangdese 92° E" passive-source seismic quasi-linear array was deployed in September 2011 for 500 km northward from the High Himalaya, across the Yarlung Zangbo Suture (YZS) and then to the Bangong–Nujiang Suture (BNS) (Fig. 1). The array comprised 46 broadband seismometers equipped with Guralp 3ESPCD sensors, and operated for 12 months in order to record sufficient teleseismic data to yield a high-resolution receiver function (RF) cross-section. The images of the crustal and upper-mantle structure of the eastern India–Tibet collision zone were obtained using common conversion point (CCP) stacks of RFs, a well-established method which has been applied in many similar studies of the Tibetan plateau (e.g. Kosarev et al., 1999; Kind et al., 2002; Kumar et al., 2006; Nábělek et al., 2009; Zhao et al., 2011). Our RF images (Figs. 2 and 3) use about double the station density available in the closest existing P-wave (Kind et al., 2002) and S-wave (Kumar et al., 2006) RF images, and have, therefore, correspondingly higher signal-to-noise ratios and lateral resolution to resolve the deformation structure of the crust and upper mantle.

The CCP RF method enhances converted S waves produced by P waves of distant earthquakes impinging on seismic interfaces (for the P-wave RFs, and vice versa for the S-wave ones). This method detects interfaces and describes their properties based on the time delays between the direct and converted waves that are proportional to the depths of the interfaces, and on the amplitudes of the converted waves that depend on the magnitudes and signs of the velocity contrasts.

We applied a visual selection process to all earthquakes recorded by the array to ensure we only used good-quality waveforms with signal-to-noise ratio above ~5. We used only teleseismic events with magnitudes $\geq$4.5 and epicentral distances greater than 30° for P-waves, from 60°–85° for S-waves, and from 85°–105° for SKS-waves. Most of these events occur to the east of the array (Supplementary Fig. A.1). A high-pass Butterworth filter of 0.02 Hz was applied to the data to suppress extremely low-frequency noise when needed. We performed time-domain iterative deconvolution (Ligorria and Ammon, 1999) in the calculation of RFs, in which the Gaussian filter factor was set to 3 for P-waves and 2 for S-waves to retain sufficient high frequency (up to 1 Hz) to image crustal and upper-mantle structure. We isolated the converted from the incident waves using the P-SH-wave-vector method, which decomposes P- and S-waves and removes the effect of the free surface by multiplying the inverse matrix of free-surface response (Reading et al., 2003) with the observed vertical, radial and transverse components of data. A free-surface response matrix calculated for surface velocities of $Vp = 5.1$ km/s and $Vs = 2.9$ km/s removed most of the effect of the free surface. All the RFs were migrated from time to depth by tracing the rays from location of each station with a layered reference model (Supplementary Table A.1), and finally stacked onto a cross-section oriented N–S, a direction perpendicular to surface geological trends as well as to expected deep-seated structures (Fig. 4) in the study region. This orientation of our cross-section is appropriate for representing structures that strike W–E. In order to retain the highest-possible spatial resolution, smoothing was minimized in the construction of the images. For stacking, all the vertical bin widths were set to 0.5 km. Horizontal bin widths for P-wave RF-CCP stacks were set to 1.0 km (Fig. 2b) or to the widths corresponding to the Fresnel zone of 1 Hz signal (Fig. 2c), and for S-wave RF-CCP stacks to 8.1 km (Fig. 3b) or 12 km (Fig. 3c).

To image steeply dipping structures at their true position, we also applied a dip-move-out (DMO) algorithm to the data (Fig. 4 and Fig. A.2). The true geometric parameters, necessary for the DMO, were measured by searching all possible plunge directions

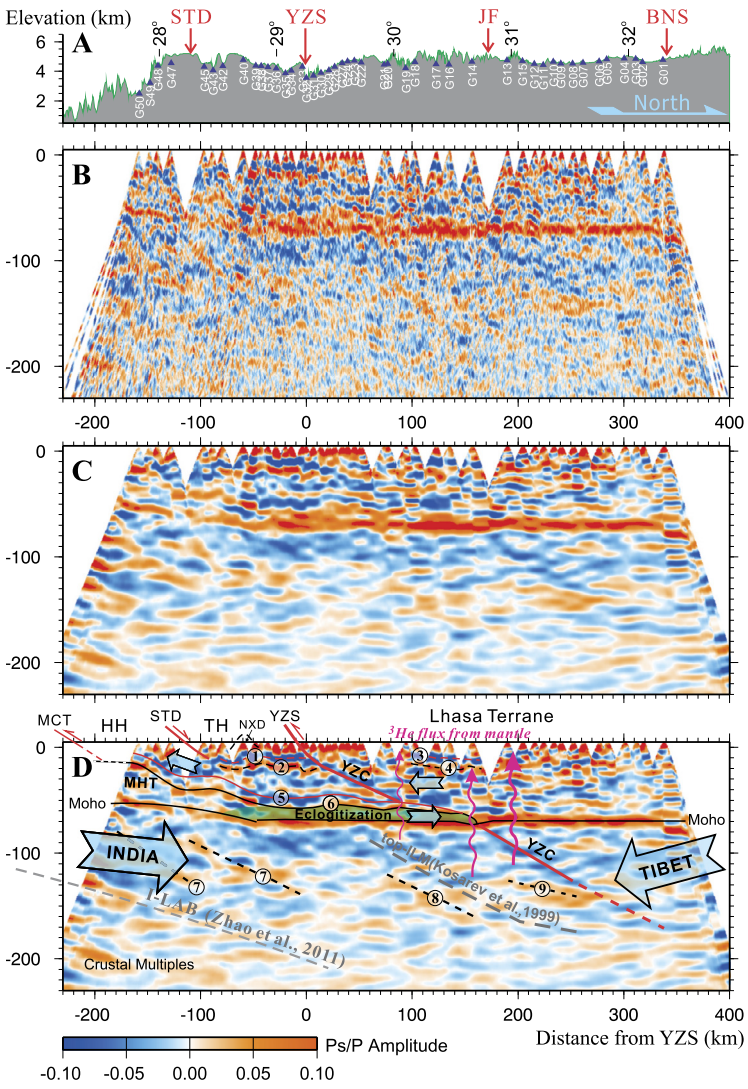

Fig. 2. Seismic image of crustal and upper-mantle structure across the eastern India–Tibet collision zone. (A) Topography and station positions along the profile. (B) Seismic cross-section constructed with a fixed horizontal stacking bin width of 1 km. Total 6310 P-wave receiver functions were migrated from time to space in a 3-D volume with a layered reference velocity model, and then projected and stacked onto a vertical cross-section aligned due north. Positive and negative amplitudes are plotted in red and blue, respectively marking interfaces with increasing and decreasing impedance with depth. Horizontal distances are referenced to station G32 (92.2094° E, 29.2540° N) at the YZS, and vertical distances are relative to sea level. (C) Seismic cross-section constructed with the horizontal bin widths corresponding to the widths of the 1 Hz Fresnel zone varied along the ray. (D) Interpretation of the main conversions, including upper-crustal low-velocity zones (between '1' and '2', '3' and '4'), lower-crustal low-velocity zone (between '5' and '6'), lower-crustal high-velocity zone (between '6' and Moho), crust–mantle boundary (Moho), Yarlung Zangbo converter (YZC), and other north dipping upper-mantle converters ('7', '8' and '9'). Dashed lines labeled Zhao et al. (2011) and Kosarev et al. (1999) are interpretations of converters made by those authors along the INDEPTH transect at ~90° E. Interfaces are shown by a solid line when the conversion is strong and by a dashed line when the conversion is weak or observed with less certainty. The green shaded area indicates our inferred eclogitized lower crust. Wiggly pink arrows denote mantle helium flux from mantle undergoing incipient melting (Klemperer et al., 2013).

and dip angles to find the optimal values that maximize the coherency of the DMO-corrected RFs in the dip direction.

3. Interpretations

3.1. Moho and lower-crustal "doublet"

A prominent positive converter (seismic impedance increases downwards) along almost the entire profile is seen at depths corresponding to the Moho defined by wide-angle seismic reflectors (Hirn and Sapin, 1984) and receiver-function inversions (Yuan et al., 1997) (Fig. 2). We thus interpret this converter to be the Moho. In the south, the Moho dips at ~7° from a depth of about 50 km under the southern High Himalaya to about 65 km beneath the Nielaxiongbo gneiss dome (NXD) (one of the North Himalayan gneiss domes – Yan et al., 2012) (Fig. 1; all depths are given below sea-level; surface elevation of ~5 km on the Tibetan Plateau must be added to Moho depths to give crustal thickness). The Moho becomes substantially horizontal at 65–72 km from ~60 km south of the YZS to ~160 km north of the YZS, in the vicinity of the Jiali fault (JF). Across this 220-km wide region, another prominent positive interface (marked '6' in Fig. 2d) lies 10–15 km above the Moho, similar to the doublet phase observed on the INDEPTH and Hi-CLIMB profiles (Kind et al., 2002; Nábělek et al., 2009). North of the JF, the Moho is a simpler, but still strong, flat and continuous, interface at a depth of about 68 km b.s.l. The high amplitude and uniform depth of the Moho beneath the northern Lhasa terrane in our study are distinctly different from the weak and complicated appearance of the Moho along the Hi-CLIMB and INDEPTH profiles (Nábělek et al., 2009; Shi et al., 2004).

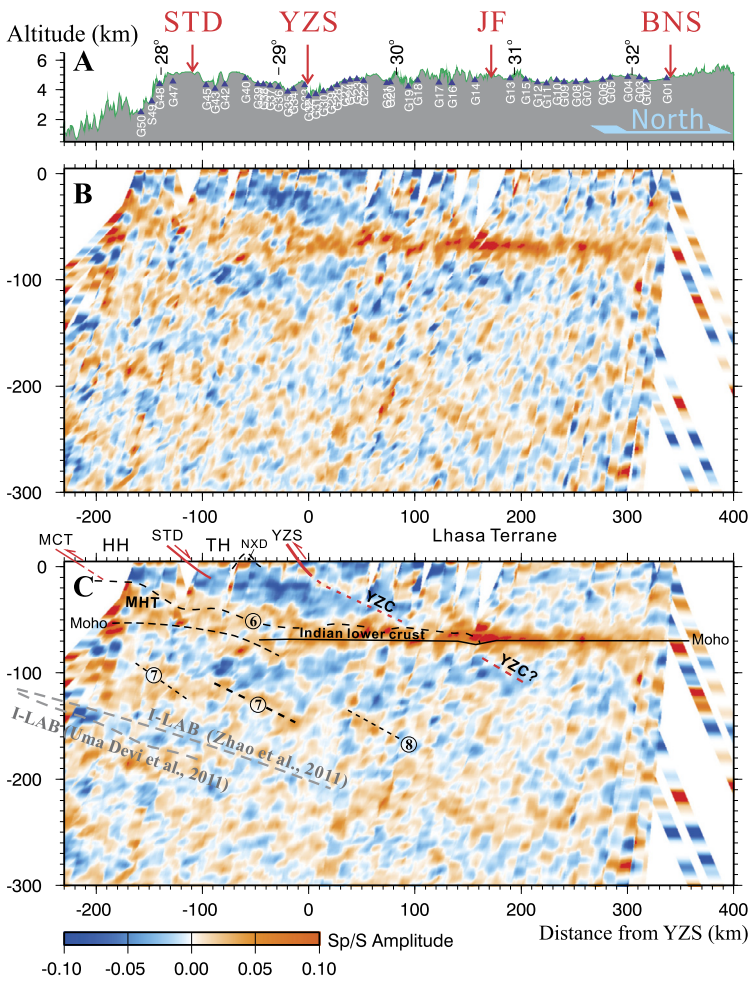

Fig. 3. S-wave receiver function image of the crustal and upper mantle structure across the eastern India–Tibet collision zone. (A) Topography and station positions along the profile. (B) Seismic cross-section constructed with a horizontal bin width of 8.1 km using 542 S-wave receiver functions. (C) Seismic cross-section constructed with a horizontal bin width of 12 km and the interpretation of the major conversion interfaces observed in the cross-section. The Moho is relatively clear, but the mantle converters such as the YZC or T-LAB, '7' and '8' are diffuse on the cross-section due to their weak impedance contrasts or gradient character at boundaries, and also due to the fewer (by a factor of 15) available S-wave data compared to the P-wave. Dashed grey lines mark the I-LAB obtained on the INDEPTH profile (Zhao et al., 2011) and in northeastern India (Uma Devi et al., 2011), aligned using latitude as reference.

The receiver-function doublet ('6' and Moho) marks a high-velocity layer above the Moho (green area in Fig. 2d) that can be tracked from the Nielaxiongbo gneiss dome south of the YZS to the vicinity of the Jiali fault. The layer is 10–15 km thick, intermediate between the 10-km doublet observed at 93–94° E (Zurek, 2008) and the 15–20 km doublet observed northwest of Lhasa (Kind et al., 2002) and at ~85° E (Nábělek et al., 2009; Wittlinger et al., 2009). Evidence of high P-wave velocity (Schulte-Pelkum et al., 2005), high density (Hetényi et al., 2007) and low Vp/Vs ratios (Wittlinger et al., 2009) have been used to suggest the presence of variable degrees of eclogitization within this doublet layer beneath the High Himalaya, Tethyan Himalaya and Lhasa block. It has previously been questioned (Wittlinger et al., 2009) whether the eclogitic doublet that was only imaged north of the YZS on the 85° E Hi-CLIMB transect (Nábělek et al., 2009) could be linked to eclogitization beneath the Tethyan Himalaya suggested in the ~87° E HIMNT experiment that did not extend north of the YZS (Schulte-Pelkum et al., 2005). Our image (Fig. 2) strongly suggests that the top of the doublet and high-velocity layer is continuous beneath the YZS, from the Jiali fault southwards at least to the North Himalaya gneiss domes (NXD) and probably to beneath the surface outcrop of the South Tibetan Detachment (STD). The brightening of this converter at increasing depths to the north of the STD may be explained as representing the gradual onset of eclogitization as Indian crust is subducted to increasing depth and pressure. The lack of a similar doublet layer north of the Jiali Fault is presumably due to the lack of a relatively uniform mafic lower crust in the northern Lhasa terrane capable of undergoing eclogitization.

The sub-horizontal geometry of the Moho beneath the YZS, in contrast to the geologically and seismically defined northward dip of the Himalayan thrusts, has been suggested to imply that the Moho beneath the YZS is a metamorphic phase change cross-cutting the dipping subduction zone (Sapin and Hirn, 1997). However, if the upper velocity increase (top of doublet, '6') is a metamorphic phase change, then the deeper velocity increase (base of doublet, Moho) cannot also be the same iso-chemical phase change and must be the lithological base of the crust. Hence Indian crust is not being subducted below the seismic Moho as a coherent unit. We follow previous workers (Hetényi et al., 2007; Nábělek et al., 2009) in inferring that the northern limit of the receiver-function doublet '6' is the northern limit of underthrust Indian crust at the Moho (Fig. 2d).

3.2. Suture zone and intra-crustal structure

Within the crust, our most interesting discovery is a prominent interface dipping north at ~20° ("Yarlung–Zangbo convert-

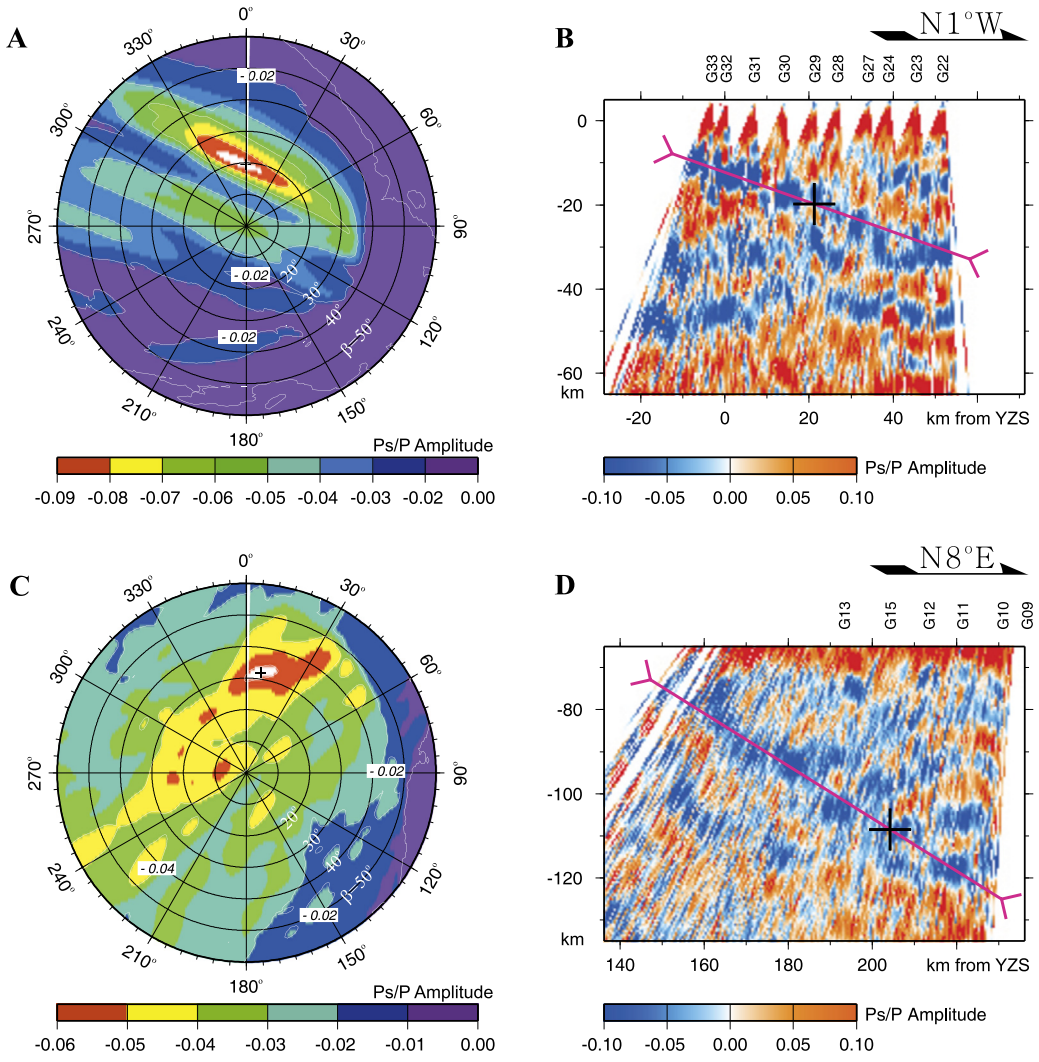

Fig. 4. Determination of the geometric parameters of the Yarlung Zangbo converter (YZC) with receiver functions. (A) Grid search of dipping parameters for the crustal section of the YZC. The stacked amplitude reaches its greatest negative amplitude (>0.09, indicated by a black cross) for a dip direction $\alpha = \text{N001}^\circ$ W, dip angle $\beta = 20^\circ$, resulting in an optimal estimate of the depth about 20 km below sea level beneath station G29 (indicated by a black cross in B). (B) Seismic cross-section for the crustal section of the YZC, migrated using dip-move-out (DMO) algorithm and the dipping parameters obtained in A. (C) Grid search of dipping parameters for the mantle section of the YZC. The most coherent amplitude (>0.06) is obtained for a dip direction $\alpha = \text{N008}^\circ$ E, dip angle $\beta = 32^\circ$, resulting in a best estimate of the depth about 109 km below sea level beneath station G15. (D) Seismic cross-section migrated with the DMO algorithm and the dipping parameters detailed in C for the mantle section of the YZC.

er" or YZC, Fig. 2) with strong negative impedance contrast (Ps/P amplitude ~10%, see Fig. 4; blue or negative polarity implies seismic impedance decreases downwards), which can be traced from close to the surface trace of the YZS to meet the receiver-function doublet 90 km further north. The YZC, and its near-parallel extension in the mantle reaching to at least 140 km depth, are robust to stacking tests and can be reproduced with synthetic models (Fig. 4 and Fig. A.2), so we are confident that these are important geological boundaries rather than artifacts of multiply converted waves. We interpret the crustal part of the YZC as the suture zone, the boundary separating Indian and Eurasian continental material. Other recent transects across southern Tibet have not imaged this feature, and their interpretive cartoons default to showing the boundary between Indian and Asian crust as a geologically implausible vertical boundary extending to 50 km depth (Nábělek et al., 2009; Nábělek and Nábělek, 2014; Priestley et al., 2008). Our image is consistent with cross-sections geologically constrained in the upper crust that show Tethyan Himalayan and orogenic prism sedimentary rocks thrust at moderate angle northwards beneath the Gangdese plutonic belt (e.g. Yin et al., 1994). The YZC suggests the same geometry may extend into the deep crust. A possibly analogous but steeper north-dipping reflection was imaged 200 km further west, on the INDEPTH reflection profile (Alsdorf et al., 1998) (Fig. A.3), and could similarly represent the suture.

Structurally beneath YZC, but still within the crust, we identify additional features of note: a negative-impedance converter '1' above a positive-impedance converter '2' ~20 km b.s.l., and a negative-impedance converter '5' above the positive-impedance lower-crustal doublet '6'.

Converters '1' and '2' are observed under NXD, one of the North Himalaya gneiss domes (Yan et al., 2012), and northwards to beneath the surface trace of the YZS, in a region where our profile follows the Cona–Sangri rift (Wu et al., 2008). This pair of converters possesses negative-over-positive polarities (impedance decrease with depth overlying an impedance increase with depth) and appears at ~ 15 km depth, similar to those pairs of converters suggested to be low-velocity zones imaged beneath grabens on the Hi-CLIMB transect (Hetényi et al., 2011). Our results indicate the low-velocity zone between these converters has a thickness ~10 km and a N–S width at least ~100 km, extending northwards to the YZC, implying this low-velocity zone may turn or root into the suture zone. INDEPTH magnetotelluric profiles across

the YZS at ~90° E and ~92° E have identified anomalously high-conductivity regions that likely represent melt as shallow as 10 km beneath the Kangmar and Nielaxiongbo North Himalayan gneiss domes (Unsworth et al., 2005; Spratt et al., 2005). However, magnetotelluric data have poor resolution of the depth to the base of highly conductive zones, thus fuelling a debate as to whether these likely zones of partial melt are continuous from ~10–65 km depth (Unsworth et al., 2005) or are confined to discontinuous zones (Spratt et al., 2005, 2012). The high-amplitude and lateral persistence of positive impedance converter '2', clearly beneath the top of the high-conductivity anomalies, strongly suggests that any magma bodies in the Tethyan Himalaya are distinct from deeper regional conductors. Converter '2' may correlate with a wide-angle reflector at 20 km depth on the INDEPTH transect at ~90° E interpreted as arising from a high-velocity slab of ophiolite beneath the Tethyan orogenic prism, lying in the footwall of the YZS (Makovsky et al., 1999). Our image further suggests that any magma bodies in the Tethyan Himalaya are also cut off by the YZS (imaged at depth as the YZC) from hypothesized magma bodies north of the YZS (Damzhung graben, northern Yadong–Gulu rift) (Nelson et al., 1996). We also observe a similar pair of converters (marked '3' and '4' in Fig. 2d) north of and structurally above the YZC. Following Hetényi et al. (2011), the low-velocity zone between '3' and '4' also likely represents partial melts; however, the mapped Cona–Sangri rift does not extend north of 29.75° N (Wu et al., 2008), so that '3' and '4' may represent shallow crustal melt outside the zones of active rifting.

South of the YZC, the most important tectonic boundary within the crust is the Main Himalayan Thrust (MHT), the subduction thrust interface along which the Indian plate now descends beneath the Himalaya and southern Tibet. The MHT was first identified beneath the southern Tethyan Himalaya at about 90° E as a velocity increase from wide-angle reflections (Hirn and Sapin, 1984) and as prominent reflections on the INDEPTH near-vertical reflection profile (Zhao et al., 1993). In contrast, the MHT was interpreted on the Hi-CLIMB profile from the High Himalaya to the Lhasa terrane as a negative impedance converter, attributed to fluids or melts trapped beneath the MHT (Nábělek et al., 2009). After a more detailed appraisal of different lithologies juxtaposed across the MHT, and the likelihood of metamorphic fluids sourced beneath the MHT and melts imaged above the MHT, Caldwell et al. (2013) suggested that the MHT may have variable polarity beneath the High Himalaya and become a positive converter further north. Recent thermo-kinematic calculations indicate that a thin low-velocity zone of partial melts may occur directly above the southern, inclined portion of the MHT due to wet melting of the orogenic prism, and above the northern, flat portion of the MHT from dehydration melting due to strain heating on the MHT (Nábělek and Nábělek, 2014). Our converters '5' and '6' parallel each other, and can be traced clearly and continuously from the High Himalaya northwards to the Jiali fault. Moreover, they possess negative-over-positive polarities, implying a low-velocity zone between them. We interpret '5' and '6' respectively as the top and the bottom of a low-velocity shear zone representing the MHT, or as a layer of partial melt immediately above the MHT (Fig. A.3c). In our interpretation, the MHT is at or immediately above the top of the doublet conversion ('6') beneath the southern Lhasa terrane and the Tethyan Himalaya. Our interpretation reconciles the previous observations (Hirn and Sapin, 1984; Zhao et al., 1993; Nábělek et al., 2009; Caldwell et al., 2013) by suggesting that the MHT may have different polarity in different regions (or on different profiles), as one or other interface is more clearly imaged. Both shear-heating within and metamorphic dehydration below the MHT can induce partial melting in the shear zone (Nábělek and Nábělek, 2014), facilitating northward subduction of the Indian lower crust and southward extrusion of the Indian middle crust, perhaps by channel flow (Beaumont et al., 2004). In the southern Tethyan Himalaya, the MHT ramps upwards to the south from a location beneath the NXD, becoming variable in conversion amplitude conceivably related to a greater patchiness in melt distribution, consistent with a decrease in electromagnetic conductivity and increase in mid-crustal seismic velocity to the south (Unsworth et al., 2005; Caldwell et al., 2009).

The crust between converter '6' and the YZC is characterized by a prominent, ~25 km thick, negative conversion on the S-wave image (Fig. 3). Although our S-wave image has inherently lower spatial resolution than the P-wave image because it was constructed with data dominated by lower frequencies, it has the advantage of not including shallow-crustal multiples. The broad negative conversion on the S-wave image may reflect a gradual decrease of impedance over a large depth span, in other words a broad low-velocity zone below the converter '2', as suggested by surface-wave dispersion results from southern Tibet (Cotte et al., 1999).

3.3. Intra-mantle converters

At mantle depths, our image of the upper mantle in both P- and S-receiver functions (Figs. 2 and 3) is dominated by north-dipping conversions, as previously observed both on INDEPTH reflection data (Alsdorf et al., 1996) and INDEPTH and Hi-CLIMB P-receiver-function images (Kosarev et al., 1999; Shi et al., 2004; Nábělek et al., 2009). The most prominent P-wave converters are the sub-Moho portion of the YZC (negative impedance), '7' and '8' (positive impedance) (Fig. 2d); all three are weak but still visible on the S receiver-function image (Fig. 3c). As is common for RF images of the shallow mantle, the converters are mostly weak, presumably weak due to small impedance contrasts in the mantle. Our interpretation of the mantle is more speculative than our results, above, for the crust, and relies on comparison with independent RF studies. Our YZC converter overlaps with the southern limit of the previously interpreted Tibetan lithosphere-asthenosphere boundary (T-LAB) (Zhao et al., 2011) and we adopt this interpretation. We similarly accept the previous interpretations of north-dipping converters on INDEPTH data, of the top of Indian lithospheric mantle beneath the Lhasa terrane (Kosarev et al., 1999) (top-ILM, Fig. 2d); and of the Indian LAB (I-LAB) beneath the High Himalaya (Uma Devi et al., 2011; Zhao et al., 2011). Top-ILM may be represented in our data by positive PRF converter '8' (Fig. 2d), and I-LAB possibly appears as diffuse negative SRF conversions (Fig. 3c) (dipping phases on the P receiver-function image at greater depths are likely crustal multiples and should not be interpreted). All these north-dipping mantle converters could be alternatively interpreted as related to diffuse deformation within the underplating Indian lithospheric mantle (ILM), similar to those interpreted on the Hi-CLIMB profile by Nábělek et al. (2009). We prefer to interpret positive converter '8' as the top of subducting ILM (Fig. 5), because it is sub-parallel to the Indian LAB imaged previously (Uma Devi et al., 2011; Zhao et al., 2011), it is close to the location interpreted by Kosarev et al. (1999), and it projects back to the inflection point of the Moho (Figs. 2d and 3c). Our interpretation is also consistent with P-wave arrival-time tomography showing subduction of the Indian lithospheric mantle at moderate angle beneath the Himalaya in our study region (Li et al., 2008). Our interpretation places the mantle suture south of the surface trace of the YZS (Fig. 5). We do not favor the possibility that YZC marks the top of Indian subducting lithosphere, and/or that Indian mantle remains attached to Indian crust to 31° N (Nábělek et al., 2009), because these hypotheses would predict a positive impedance contrast for YZC, would imply more than doubling the thickness of the subducting mantle lithosphere to ~200 km at 31° N, and would be inconsistent with mantle-derived geothermal helium emissions observed

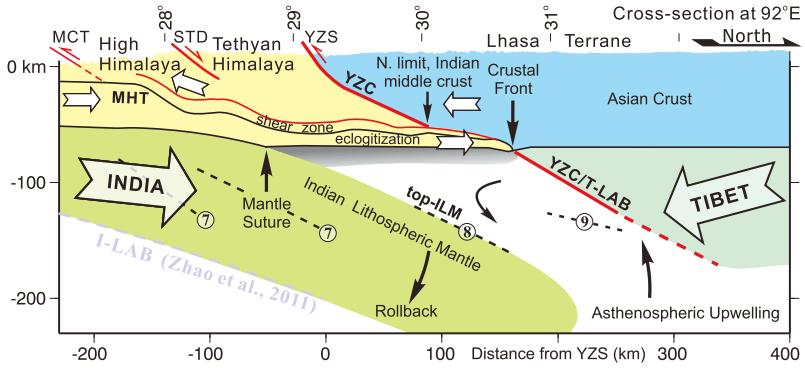

Fig. 5. Our preferred interpretive cross section of the India–Tibet collision at 92° E. Indian lower crust (yellow) underplates southern Tibet up to ~31° N, but Indian lithospheric mantle (ILM) (green) detaches from the lower crust at ~ 60 km south of the surface trace of the Yarlung Zangbo suture (YZS). Asthenospheric upwelling is caused by the roll-back or delamination of ILM. Indian middle crust (yellow) extrudes southwards due to the back-stop of Lhasa terrane crust (blue). A thin mantle lid (grey-shading) exists above the mantle wedge (explaining the observed high-amplitude Moho conversion), possibly formed from a mix of Indian and Tibetan mantle, or cooling of asthenospheric material.

north of 30° N (Hoke et al., 2000). Instead, we suggest that negative converter YZC represents the Tibetan LAB (T-LAB) beneath the Lhasa terrane, separated from the subducting Indian lithosphere by an asthenospheric mantle wedge.

The sub-Moho portion of YZC is robustly imaged by P-wave RFs (Figs. 4 and A.2) and has a Ps/P amplitude of c. 6%, consistent with other observations of the LAB (e.g. Fischer et al., 2010). The LAB is generally thought of as a thermal boundary layer (transition from conductive to convective heat transport) and not an abrupt velocity boundary, implying that it should be hard to image. However, in numerous studies worldwide, both Sp and Ps receiver functions provide evidence of relatively sharp velocity gradients interpreted as the LAB that are incompatible with an origin only as a thermal boundary layer (Fischer et al., 2010). Recent body-wave tomography utilizing newer array data and newer finite-frequency techniques (Ren and Shen, 2008; Liang et al., 2012) has found variable seismic velocities in the uppermost mantle of southeast Tibet, including low velocities beneath the Cona–Sangri rift at 92° E. The low upper-mantle velocities are interpreted as asthenospheric upwelling due to lithospheric delamination beneath the rift (Ren and Shen, 2008) or around a fragmenting subducting Indian slab (Liang et al., 2012). Our imaging of the dipping boundaries we interpret as top Indian lithospheric mantle and Tibetan LAB allow us to infer the presence of an asthenospheric mantle wedge south of the Jiali fault (JF), but are admittedly along a single 2D profile across a complex region. The recognition of a mantle wedge in the study area can help to explain the flux of mantle helium observed in the northern Lhasa terrane (Hoke et al., 2000; Klemperer et al., 2013), and also offers a source of water required for complete eclogitization of the lower crust (Leech, 2001). It is noteworthy that our inferred region of eclogitization is immediately above our inferred mantle wedge.

Our image shows an additional positive converter below the sub-Moho portion of the YZC ('9', Fig. 2d) in the mantle. This converter is within our inferred mantle wedge. We speculate it could represent a fragment of eclogitized Indian lower crust delaminated into upper mantle. Our image (Fig. 2d) shows the Indian lower crust has underthrust the uniform prolongation of the YZS at the base of the crust by only ~50 km. The underthrusting rate of Indian lower crust under southern Tibet is estimated at 1.6 cm/year (Wang et al., 2001). This suggests that the observed geometry has developed in less than 3.5 Ma, far less than the time since collision. Therefore it is plausible to conjecture that a large portion of Indian lower crust has delaminated or recycled into the mantle.

The mantle converters '7' on the P-wave image (Fig. 2d) and S-wave image (Fig. 3c) are geometrically similar to conversions observed beneath the High Himalaya on the INDEPTH and Hi-CLIMB profiles and may indicate active deformation (Alsdorf et al., 1996; Nábělek et al., 2009).

4. Discussion

The crustal portion of the YZC extending from upper to lower crust implies the lack of long-distance north-south middle crustal flow between the Tethyan Himalaya and the Lhasa terrane. The hypothesized channel-flows of Indian middle crust extruding southwards from Tibet (Beaumont et al., 2004) are limited in our study region by the YZC to the southernmost portion of the Lhasa terrane. High-reflectivity, high-conductivity "bright spots" imaged structurally above YZC in the Yangbajain graben on INDEPTH profiles (Nelson et al., 1996) are unrelated to southward channel-flow extrusion of the High Himalaya (Klemperer, 2006). Surface-wave dispersion analyses indicate that a pronounced low-velocity layer is present in the middle-to-lower crust (20–65 km depth) of the southern Lhasa terrane south of ~30° N (Cotte et al., 1999), whereas the northern Lhasa terrane north of ~30° N has a thinner, shallower (15–25 km b.s.l.) and lower-magnitude low-velocity zone (Rapine et al., 2003; Klemperer, 2006), suggesting the existence of a stronger middle-to-lower crust for the northern region. Geological observations indicate the Lhasa terrane has undergone relatively little N–S shortening during the Cenozoic (Yin et al., 1994; Murphy et al., 1997), supporting our interpretation of stronger Tibetan crust north of the YZC that can be considered as a back-stop to crustal subduction. A discordant relationship between the dipping suture converter (YZC) and the doublet converter ('6') at the base of the crust suggests the high-velocity Indian lower crust is continuing to inject up to 50 km further north, even while Indian upper crust is forming a crustal-scale orogenic wedge against the back-stop of Lhasa terrane crust (Fig. 5). The angular relationship between the suture and the Indian lower crust means that Indian upper- and middle-crust is not being subducted to sub-Moho depths, but must be returned upwards and southwards, perhaps as a channel flow (Beaumont et al., 2004) albeit limited to the southernmost Lhasa block, south of ~30° N. Predictions of numerical models of channel flows depend on many critical parameters (Beaumont et al., 2004), including the location of the "mantle suture".

We interpret the sub-Moho portion of the YZC to be a manifestation of the Tibetan lithosphere–asthenosphere boundary (T-LAB), bounding an asthenospheric window resulting from roll-back or delamination of Indian lithospheric mantle (ILM). Geological compilations indicate that post-collisional ultrapotassic and adakitic magmatism migrated southwards across the Lhasa terrane from ~26–10 Ma, leading Chung et al. (2005) to infer convective re-

moval of a thickened Lhasa-block lithospheric root at ~26 Ma to form an asthenospheric window. Volcanism is unknown in southern Tibet after 10 Ma, often interpreted as representing a shut-off of the asthenospheric window by resumed horizontal underthrusting of Indian lithosphere (Chung et al., 2005) in the geometry suggested by the Hi-CLIMB image at 85° E (Nábělek et al., 2009). The asthenospheric mantle wedge we interpret (Fig. 5) could either be relict since the removal of a lithospheric root at ~26 Ma, or could be a newly developed roll-back or delamination of Indian lithospheric mantle (ILM). The lack of recent volcanic activity in southern Tibet may most simply be attributed to a waning supply of mantle melt since a ~26 Ma delamination, so that any mantle-derived melts are trapped in the crust.

We suggest that the Indian mantle lithosphere detaches from Indian lower crust at the Moho inflection point under the Tethyan Himalaya, placing the mantle suture ~50 km south of the surface trace of the YZS in our study region. Our suggested mantle suture at 92° E is ~70 km south of the proposed mantle suture that is close to the surface trace of the YZS at ~90° E along the INDEPTH profile (Kosarev et al., 1999; Zhao et al., 2011), and ~250 km south of the suggested 31° N northern limit of underthrusting Indian lower crust at ~85° E along the Hi-CLIMB profile (Nábělek et al., 2009). We believe that the geometry of subduction of Indian lower lithosphere beneath southern Tibet changes along strike. This interpretation is supported by several previous datasets: First, previous P-wave arrival time tomography has also resolved a change of the Indian mantle lithosphere from subhorizontal underthrusting beneath the entire plateau in the west to steep subduction under the southern margin of the Himalaya in the central–eastern Tibet (Li et al., 2008), despite both our and Hi-CLIMB results indicating that Indian lower crust has subhorizontally underthrust to a similar northern extent at ~31° N along the two profiles. Second, the eastern Lhasa terrane is characterized by more negative Bouguer gravity anomalies than the western one (He et al., 2014), implying a less dense upper mantle in eastern Tibet. Third, post-collisional magmatism and porphyry metallogeny show less contamination by Indian mantle lithosphere and an increased asthenospheric component in the eastern Gangdese as compared to the western Gangdese belt (Hou et al., 2006; Hou and Cook, 2009; Zhao et al., 2009), suggesting a change from sub-horizontal underthrusting of Indian mantle lithosphere in the west to steeper subduction in the east. Our interpretation fits other previous results, including gravity modeling (Jin et al., 1996) and observations of mantle-derived helium (Hoke et al., 2000; Klemperer et al., 2013).

5. Conclusions

We have constructed receiver-function images of the crustal and upper-mantle structure in the eastern India–Tibet collision zone at 92° E, which allow us to achieve a better understanding of crustal deformation and mantle tectonic processes in the southern Tibetan plateau.

Our images show a prominent converter dipping ~20° N from near-surface to ~150 km depth that we interpret as the Yarlung–Zangbo Suture zone (YZS) in the crust and the Tibetan lithosphere-asthenosphere boundary (T-LAB) in the mantle. Our results suggest that the hypothesized channel-flows of Indian middle crust extruding southwards from Tibet are most likely limited to the southernmost portion of the Lhasa terrane. Our results also show sub-parallel converters in the mantle that we associate with the subduction of Indian lithospheric mantle, detaching from underthrusting Indian crust at the mantle suture ~50 km south of the surface trace of the YZS.

Our results in this study together with those obtained by the Hi-CLIMB transect, as well as body-wave and surface-wave tomography, and potential-field and geochemical data, lead us to conclude that the geometry of subduction of Indian lower lithosphere beneath southern Tibet changes along strike. In contrast, Indian crust seems to penetrate a fairly uniform distance beneath Tibet over a large sector of the orogen at least from 85° to 92° E, to the "Indian crustal front" >150 km north of the YZS (Fig. 5). Thus the underplating of Indian crust beneath the Lhasa Terrane may be controlled by the geometry of collision as recorded by the YZS at the surface, whereas progressive detachment of Indian mantle lithosphere from Indian crust may be related to stresses at the eastern syntaxis associated with ongoing subduction of the Burma plate.

Acknowledgements

This research was funded by the Chinese Geological Survey (1212011120185), and the National Natural Science Foundation (41374109) of China. We are grateful to two anonymous reviewers for providing us a lot of constructive comments and suggestions which have greatly improved the manuscript. We used the GMT software package (Wessel and Smith, 1998) for production of most figures.

Appendix A. Supplementary material

Supplementary material related to this article can be found online at http://dx.doi.org/10.1016/j.epsl.2014.12.055.

References

Alsdorf, D., Brown, L.D., Nelson, K.D., 1996. Possible upper mantle reflection fabric on seismic profiles from the Tethyan Himalaya: identification and tectonic interpretation. J. Geophys. Res. 101, 25305–25320.

Alsdorf, D., Brown, L., Nelson, K.D., Makovsky, Y., Klemperer, S., Zhao, W., 1998. Crustal deformation of the Lhasa terrane, Tibet plateau from Project INDEPTH deep seismic reflection profiles. Tectonics 17, 501–519.

Argand, E., 1924. La tectonique de l'Asie. Int. Geol. Congr. Rep. Sess. 13, 170–372.

Beaumont, C., Jamieson, R.A., Nguyen, M.H., Medvedev, S., 2004. Crustal channel flows: 1. Numerical models with applications to the tectonics of the Himalayan–Tibetan orogen. J. Geophys. Res. 109, B06406.

Caldwell, W.B., Klemperer, S.L., Rai, S.S., Lawrence, J.F., 2009. Partial melt in the upper-middle crust of the northwest Himalaya revealed by Rayleigh wave dispersion. Tectonophysics 477, 58–65. http://dx.doi.org/10.1016/j.tecto.2009.01.013.

Caldwell, W.B., Klemperer, S.L., Lawrence, J.F., Rai, S.S., 2013. Characterizing the Main Himalayan Thrust in the Garhwal Himalaya, India with receiver function CCP stacking. Earth Planet. Sci. Lett. 367, 15–27. http://dx.doi.org/10.1016/j.epsl.2013.02.009.

Capitanio, F.A., Morra, G., Goes, S., Weinberg, R.F., Moresi, L., 2010. India–Asia convergence driven by the subduction of the Greater Indian continent. Nat. Geosci. 3, 136–139.

Chung, S.L., Chu, M.F., Zhang, Y., Xie, Y., Lo, C.H., Lee, T.Y., Lan, C.Y., Li, X.H., Zhang, Q., Wang, Y., 2005. Tibetan tectonic evolution inferred from spatial and temporal variations in post-collisional magmatism. Earth-Sci. Rev. 68, 173–196.

Clark, M.K., Royden, L.H., 2000. Topographic ooze: building the eastern margin of Tibet by lower crustal flow. Geology 28, 703–706.

Cotte, N., Pedersen, H., Campillo, M., Mars, J., Ni, J.F., Kind, R., Sandvol, E., Zhao, W., 1999. Determination of the crustal structure in southern Tibet by dispersion and amplitude analysis of Rayleigh waves. Geophys. J. Int. 138, 809–819.

Dewey, J.F., Burke, K., 1973. Tibetan, Variscan, and Precambrian basement reactivation: products of continental collision. J. Geol. 81, 683–692.

England, P., Houseman, G., 1989. Extension during continental convergence, with application to the Tibetan Plateau. J. Geophys. Res. 94, 17561–17579.

Fischer, K.M., Ford, H.A., Abt, D.L., Rychert, C.A., 2010. The lithosphere–asthenosphere boundary. Annu. Rev. Earth Planet. Sci. 38, 551–575.

He, R., Liu, G., Golos, E., Gao, R., Zheng, H., 2014. Isostatic gravity anomaly, lithospheric scale density structure of the northern Tibetan plateau and geodynamic causes for potassic lava eruption in Neogene. Tectonophysics. http://dx.doi.org/10.1016/j.tecto.2014.04.047.

Hetényi, G., Cattin, R., Brunet, F., Bollinger, L., Vergne, J., Nábělek, J.L., Diament, M., 2007. Density distribution of the India plate beneath the Tibetan plateau: geophysical and petrological constraints on the kinetics of lower-crustal eclogitization. Earth Planet. Sci. Lett. 264, 226–244.

Hetényi, G., Vergne, J., Bollinger, L., Cattin, R., 2011. Discontinuous low-velocity zones in southern Tibet question the viability of the channel flow model. Geol. Soc. (Lond.) Spec. Publ. 353, 99–108.
Hirn, A., Sapin, M., 1984. The Himalayan zone of crustal interaction: suggestions from explosion seismology. Ann. Geophys. 2, 123–130.
Hoke, L., Lamb, S., Hilton, D.R., Poreda, R.J., 2000. Southern limit of mantle-derived geothermal helium emissions in Tibet: implications for lithospheric structure. Earth Planet. Sci. Lett. 180, 297–308. http://dx.doi.org/10.1016/S0012-821X(00)00174-6.
Hou, Z., Cook, N.J., 2009. Metallogenesis of the Tibetan collisional orogen: a review and introduction to the special issue. Ore Geol. Rev. 36, 2–24.
Hou, Z.Q., Zhao, Z.D., Gao, Y.F., Yang, Z.M., Jiang, W., 2006. Tearing and diachronal subduction of the Indian continental slab: evidence from Cenozoic Gangdese volcano-magmatic rocks in south Tibet. Acta Petrol. Sin. 22, 761–774.
Jin, Y., McNutt, M.K., Zhu, Y.S., 1996. Mapping the descent of Indian and Eurasian plates beneath the Tibetan Plateau from gravity anomalies. J. Geophys. Res. 101, 11275–11290.
Kind, R., Yuan, X., Saul, J., Nelson, D., Sobolev, S.V., Mechie, J., Zhao, W., Kosarev, G., Ni, J., Achauer, U., Jiang, M., 2002. Seismic images of crust and upper mantle beneath Tibet: evidence for Eurasian plate subduction. Science 298, 1219–1221. http://dx.doi.org/10.1126/science.1078115.
Klemperer, S.L., 2006. Crustal flow in Tibet: geophysical evidence for the physical state of Tibetan lithosphere, and inferred patterns of active flow. Geol. Soc. (Lond.) Spec. Publ. 268, 39–70. http://dx.doi.org/10.1144/GSL.SP.2006.268.01.03.
Klemperer, S.L., Kennedy, B.M., Sastry, S.R., Makovsky, Y., Harinarayana, T., Leech, M.L., 2013. Mantle fluids in the Karakoram fault: helium isotope evidence. Earth Planet. Sci. Lett. 366, 59–70.
Kosarev, G., Kind, R., Sobolev, S.V., Yuan, X., Hanka, W., Oreshin, S., 1999. Seismic evidence for a detached Indian lithospheric mantle beneath Tibet. Science 283, 1306–1309. http://dx.doi.org/10.1126/science.283.5406.1306.
Kumar, P., Yuan, X., Kind, R., Ni, J., 2006. Imaging the colliding Indian and Asian lithospheric plates beneath Tibet. J. Geophys. Res. 111, B06308.
Leech, M.L., 2001. Arrested orogenic development: eclogitization, delamination, and tectonic collapse. Earth Planet. Sci. Lett. 185, 149–159.
Leech, M.L., Singh, S., Jain, A.K., Klemperer, S.L., Manickavasagam, R.M., 2005. The onset of India–Asia continental collision: early, steep subduction required by the timing of UHP metamorphism in the western Himalaya. Earth Planet. Sci. Lett. 234, 83–97. http://dx.doi.org/10.1016/j.epsl.2005.02.038.
Li, C., Van der Hilst, R.D., Meltzer, A.S., Engdahl, E.R., 2008. Subduction of the Indian lithosphere beneath the Tibetan Plateau and Burma. Earth Planet. Sci. Lett. 274, 157–168. http://dx.doi.org/10.1016/j.epsl.2008.07.016.
Liang, X., Sandvol, E., Chen, Y.J., Hearn, T., Ni, J., Klemperer, S., Shen, Y., Tilmann, F., 2012. A complex Tibetan upper mantle: a fragmented Indian slab and no south-verging subduction of Eurasian lithosphere. Earth Planet. Sci. Lett. 333–334, 101–111. http://dx.doi.org/10.1016/j.epsl.2012.03.036.
Ligorria, J., Ammon, C.J., 1999. Iterative deconvolution and receiver function estimation. Bull. Seismol. Soc. Am. 89, 1395–1400.
Makovsky, Y., Klemperer, S.L., Ratschbacher, L., Alsdorf, D., 1999. Midcrustal reflector on INDEPTH wide-angle profiles: an ophiolite slab beneath the India–Asia suture in southern Tibet? Tectonics 18, 793–808. http://dx.doi.org/10.1029/1999TC900022.
Molnar, P., Tapponnier, P., 1975. Cenozoic tectonics of Asia: effects of a continental collision. Science 189, 419–426.
Murphy, M.A., Yin, A., Harrison, T.M., Du, S.B., Chen, Z., Ryerson, F.J., Kidd, W.S.F., Wang, X., Zhou, X., 1997. Did the Indo-Asian collision alone create the Tibetan plateau? Geology 25, 719–722.
Nábělek, P., Nábělek, J., 2014. Thermal characteristics of the Main Himalaya Thrust and the Indian lower crust with implications for crustal rheology and partial melting in the Himalaya orogen. Earth Planet. Sci. Lett. 395, 116–123.
Nábělek, J., György, H., Vergne, J., Sapkota, S., Kafle, B., Jiang, M., Su, H., Chen, J., Huang, B.S., Hi-CLIMB Team, 2009. Underplating in the Himalaya–Tibet collision zone revealed by the Hi-CLIMB experiment. Science 325, 1371–1374. http://dx.doi.org/10.1126/science.1167719.
Nelson, K.D., et al., 1996. Partially molten middle crust beneath Southern Tibet: synthesis of Project INDEPTH results. Science 274, 1684–1688. http://dx.doi.org/10.1126/science.274.5293.1684.
Ni, J., Barazangi, M., 1983. High-frequency seismic wave propagation beneath the Indian Shield, Himalayan Arc, Tibetan Plateau and surrounding regions: high uppermost mantle velocities and efficient S_n propagation beneath Tibet. Geophys. J. Int. 72, 665–689.
Powell, C.M., Conaghan, P.J., 1973. Plate tectonics and the Himalayas. Earth Planet. Sci. Lett. 20, 1–12.
Priestley, K., Jackson, J., McKenzie, D., 2008. Lithospheric structure and deep earthquakes beneath India, the Himalaya and southern Tibet. Geophys. J. Int. 172, 345–362. http://dx.doi.org/10.1111/j.1365-246X.2007.03636.x.
Rapine, R., Tilmann, F., West, M., Ni, J., Rodgers, A., 2003. Crustal structure of northern and southern Tibet from surface wave dispersion analysis. J. Geophys. Res. 108, 2120. http://dx.doi.org/10.1029/2001JB000445.
Reading, A., Kennett, B., Sambridge, M., 2003. Improved inversion for seismic structure using transformed, S-wave vector receiver functions: removing the effect of the free surface. Geophys. Res. Lett. 30, 1981. http://dx.doi.org/10.1029/2003GL018090.
Ren, Y., Shen, Y., 2008. Finite frequency tomography in southeastern Tibet: evidence for the causal relationship between mantle lithosphere delamination and the north–south trending rifts. J. Geophys. Res. 113, B10316. http://dx.doi.org/10.1029/2008JB005615.
Sapin, M., Hirn, A., 1997. Seismic structure and evidence for eclogitization during the Himalayan convergence. Tectonophysics 273, 1–16.
Schulte-Pelkum, V., Monsalve, G., Sheehan, A., Pandey, M.R., Sapkota, S., Bilham, R., Wu, F., 2005. Imaging the Indian subcontinent beneath the Himalaya. Nature 435, 1222–1225. http://dx.doi.org/10.1038/nature03678.
Shi, D., Zhao, W., Brown, L., Nelson, D., Zhao, X., Kind, R., Ni, J., Xiong, J., Mechie, J., Guo, J., Klemperer, S., Hearn, T., 2004. Detection of southward intracontinental subduction of Tibetan lithosphere along the Bangong–Nujiang suture by P-to-S converted waves. Geology 32, 209–212.
Spratt, J.E., Jones, A.G., Nelson, K.D., Unsworth, M.J., INDEPTH MT Team, 2005. Crustal structure of the India–Asia collision zone, southern Tibet, from INDEPTH MT investigations. Phys. Earth Planet. Inter. 150, 227–237.
Spratt, J.E., Jones, A.G., Klemperer, S., Wei, W., the INDEPTH MT Team, 2012. Discontinuous electrical conductivity across the Yarlung–Zangbo Suture, Southern Tibet, from re-analysis of INDEPTH MT data. In: 34th Session of the International Geological Congress (IGC). Brisbane, Australia.
Tapponnier, P., Xu, Z., Roger, F., Meyer, B., Arnaud, N., Wittlinger, G., Yang, J., 2001. Oblique stepwise rise and growth of the Tibet Plateau. Science 294, 1671–1677. http://dx.doi.org/10.1126/science.105978.
Uma Devi, E., Kumar, P., Ravi Kumar, M., 2011. Imaging the Indian lithosphere beneath the eastern Himalayan region. Geophys. J. Int. 187, 631–641.
Unsworth, M.J., Jones, A.G., Wei, W., Marquis, G., Gokarn, S.G., Spratt, J.E., Bedrosian, P., Booker, J., Chen, L., Clarke, G., Li, S., Lin, C., Deng, M., Jin, S., Solon, K., Tan, H., Ledo, J., Roberts, B., 2005. Crustal rheology of the Himalaya and southern Tibet inferred from magnetotelluric data. Nature 438, 78–81. http://dx.doi.org/10.1038/nature04154.
Wang, Q., Zhang, P.Z., Freymueller, J.T., Bilham, R., Larson, K.M., Lai, X.A., You, X.Z., Niu, Z.J., Wu, J.C., Li, Y.X., Liu, J.N., Yang, Z.Q., Chen, Q.Z., 2001. Present-day crustal deformation in china constrained by global positioning system measurements. Science 294, 574–577. http://dx.doi.org/10.1126/science.1063647.
Wessel, P., Smith, W.H.F., 1998. New, improved version of genericmapping tools released. Eos 79, 579.
Wittlinger, G., Farra, V., Hetényi, G., Vergne, J., Nábělek, J., 2009. Seismic velocities in southern Tibet lower crust: a receiver function approach for eclogite detection. Geophys. J. Int. 177, 1037–1049.
Wu, Z.H., Zhang, Y.S., Hu, D.G., Zhao, X.T., Ye, P.S., 2008. The Quaternary normal faulting of the Cona–Oiga rift. Seismol. Geol. 30, 144–160.
Yan, D.P., Zhou, M.F., Robinson, P.T., Grujic, D., Malpas, J., Kennedy, A., Reynolds, P.H., 2012. Constraining the mid-crustal channel flow beneath the Tibetan Plateau: data from the Nielaxiongbo gneiss dome, SE Tibet. Int. Geol. Rev. 54, 615–632.
Yang, Y., Ritzwoller, M.H., Zheng, Y., Shen, W., Levshin, A.L., Xie, Z., 2012. A synoptic view of the distribution and connectivity of the mid-crustal low velocity zone beneath Tibet. J. Geophys. Res. 117, B04303. http://dx.doi.org/10.1029/2011JB008810.
Yin, A., Harrison, T.M., 2000. Geologic evolution of the Himalayan–Tibetan orogen. Annu. Rev. Earth Planet. Sci. 28, 211–280.
Yin, A., Harrison, T.M., Ryerson, F.J., Wenji, C., Kidd, W.S.F., Copeland, P., 1994. Tertiary structural evolution of the Gangdese thrust system, southeastern Tibet. J. Geophys. Res. 99, 18175–18201.
Yuan, X., Ni, J., Kind, R., Mechie, J., Sandvol, E., 1997. Lithospheric and upper mantle structure of southern Tibet from a seismological passive source experiment. J. Geophys. Res. 102, 27491–27500.
Zhao, W., Nelson, K.D., Project INDEPTH Team, 1993. Deep seismic reflection evidence for continental underthrusting beneath southern Tibet. Nature 366, 557–559. http://dx.doi.org/10.1038/366557a0.
Zhao, W., Kumar, P., Mechie, J., Kind, R., Meissner, R., Wu, Z., Shi, D., Su, H., Xue, G., Karplus, M., Tilmann, F., 2011. Tibetan plate overriding the Asian plate in central and northern Tibet. Nat. Geosci. 4, 870–873. http://dx.doi.org/10.1038/NGEO1309.
Zhao, Z., Mo, X., Dilek, Y., Niu, Y., DePaolo, D.J., Robinson, P., Zhu, D., Sun, C., Dong, G., Zhou, S., Luo, Z., Hou, Z., 2009. Geochemical and Sr–Nd–Pb–O isotopic compositions of the post-collisional ultrapotassic magmatism in SW Tibet: petrogenesis and implications for India intra-continental subduction beneath southern Tibet. Lithos 113, 190–212.
Zurek, B., 2008. The evolution and modification of continental lithosphere, dynamics of 'indentor corners' and imaging the lithosphere across the eastern syntaxis of Tibet. PhD thesis. Lehigh University, pp. viii+250.

Supplementary Materials for

Receiver Function Imaging of Crustal Suture, Steep Subduction, and Mantle Wedge in the Eastern India-Tibet Continental Collision Zone

Danian Shi, Zhenhan Wu, Simon L. Klemperer, Wenjin Zhao, Guangqi Xue, Heping Su

The reference velocities employed for the migration of receiver functions are listed in Table A.1. All the earthquakes used for the analysis are shown in Fig. A.1. Synthetic tests of the geometric parameters resolved for the Yarlung Zangbo converter are shown in Fig. A.2. A comparison of our receiver function cross-section with the INDEPTH reflection profile and different interpretations of the Main Himalayan Thrust (MHT) are shown in Fig. A.3.

Table A.1. Velocity model used in the migration from time to depth in the common conversion point (CCP) stack of receiver functions

Layer#	Vp (km/s)	Vs (km/s)	Depth of the top interface (km b.s.l.)
1	6.2000	3.6000	-9
2	8.1000	4.4700	70
3	8.0500	4.5000	120
4	8.2375	4.5135	165
5	8.3000	4.5200	210
6	8.5738	4.6525	260
7	8.7562	4.7395	310
8	8.9387	4.8265	360
9	9.1950	4.9700	410
10	9.6120	5.2290	460
11	9.7800	5.3350	510
12	9.9480	5.4410	560
13	10.1160	5.5470	610
14	10.4950	5.7750	660

Figures and legends

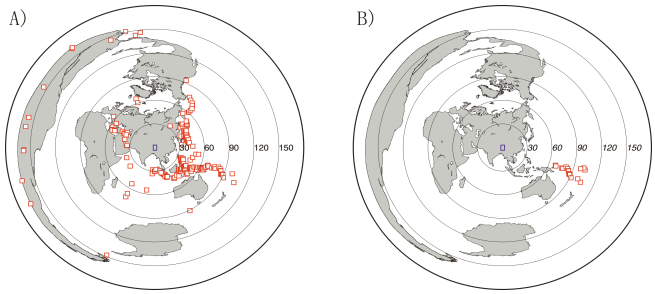

Fig. A.1. Distribution of earthquakes used to construct P-wave (A) and S-wave (B) receiver function images. Red rectangles show the locations of earthquakes used. The maps are centered at the center of the seismic array (92°E, 30°N) with a blue rectangle denotes the location of Fig. 1.

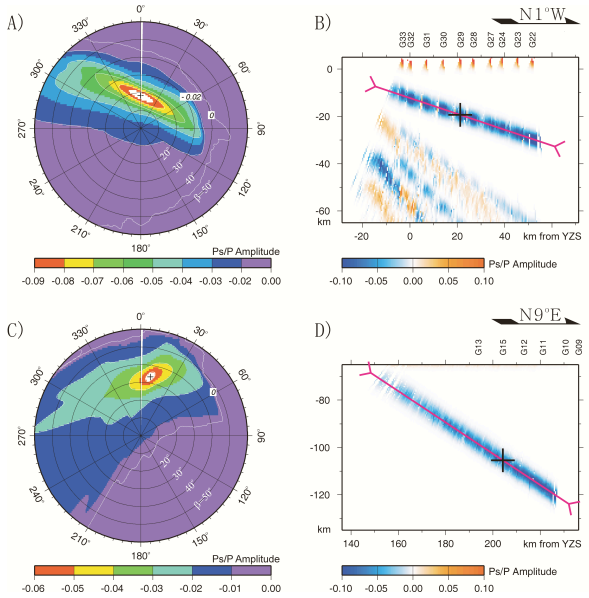

Fig. A.2. Test of the geometric parameters of the Yarlung Zangbo converter (YZC) with synthetic receiver functions calculated with the raysum code (Frederiksen & Bostock, 2000). (A) Grid-search result yields a dip direction α=N001°W, dip angle β=19°, and a best estimate of the depth of about 19 km below sea level beneath the station G29. (B) Synthetic seismic cross-section for the crustal section of the YZC obtained using a model with the geometric parameters resolved and detailed in Fig. 4A, migrated using the DMO method and the dipping parameters retrieved in A. (C) Grid-search result yields a dip direction α=N009°E, dip angle β=33°, and a best estimate of the depth of about 105 km below sea level beneath the station G15. (D) Synthetic seismic cross-section for the mantle section of the YZC created with the parameters detailed in Fig. 4C, migrated with the dipping parameters retrieved in C.

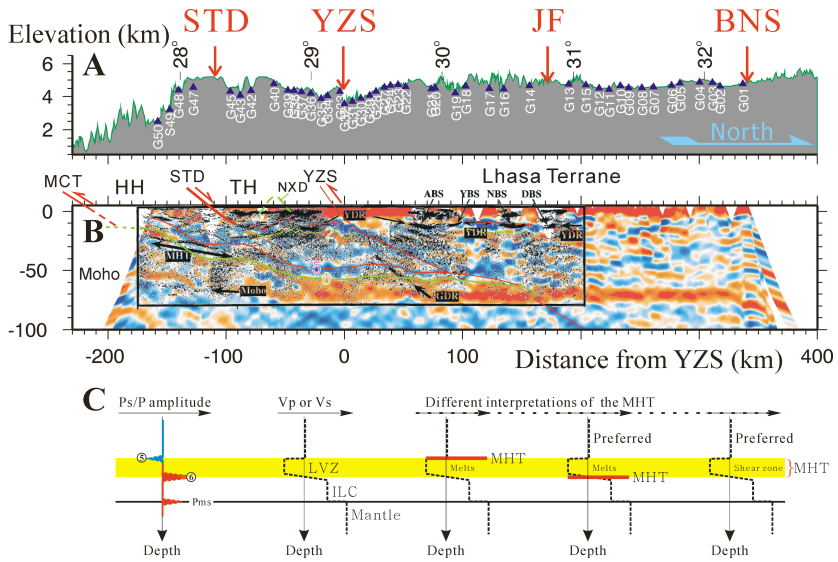

Fig. A.3. (A) Topography and station positions along the profile. (B) Comparison of our P-wave receiver function cross-section with the INDEPTH reflection profile (Alsdorf et al., 1998) aligned using latitude as reference. A north-dipping reflector labeled 'GDR' (Gangdese deep reflection) was resolved on the INDEPTH reflection profile, about 200 km to the west of our cross-section (see Fig. 1). We interpret the GDR and the YZC as belonged to an identical structure, because both of them project to the surface close to the outcrop at surface trace of the YZS [or YTS in the terminology of Makovsky et al., 1999]. The change in dip observed between the GDR and the YZC may suggest a geometrical variation along the east-west direction. The MHT on the reflection profile corresponds well to a middle-lower crustal low-velocity zone (LVZ; between '5' and '6') on the receiver function cross-section. The Moho on the reflection profile is only visible beneath the High Himalaya (HH), and disappears where the lower crust 'doublet' (marked '6') appears on the receiver function cross-section. Our positive converter '2' corresponds to the wide-angle reflection shown as a green dashed line, inferred to be an ophiolitic body within the suture zone (Makovsky et al., 1999). (C) Schematic amplitude-depth and velocity-depth profiles and different interpretations of the MHT. Alternate interpretations either 1) trace the negative converter (top of the LVZ) as the MHT by ascribing the LVZ to be melts trapped below the MHT (e.g. Nábělek et al., 2009), 2) trace the positive converter (bottom of the LVZ) as the MHT by assuming the LVZ containing melts sourced beneath the MHT (e.g. Caldwell et al., 2013), or 3) take the entire LVZ as the MHT by assuming the LVZ represents a shear zone. Recent thermo-kinematic calculations show that crustal melts may occur directly above the eclogitic Indian Lower Crust (ILC), separated by the MHT (Nábělek & Nábělek, 2014). The second interpretation (MHT=base LVZ) may best fit the inclined portion of the MHT, due to wet melting induced by dehydration of the underthrusting Indian lithosphere. The third interpretation (thick MHT shear zone=LVZ) may best fit the flat portion of the MHT, where the underlying ILC is supposed to be anhydrous eclogite, and the LVZ is most likely a mechanical weak zone resulting from shearing or strain heating of the MHT itself (Nábělek & Nábělek, 2014). The bottom of the MHT and the top of the ILC can not be separated, and correspond to a compound conversion marked '6' in our interpretation.

References

A.1. Frederiksen, A.W., Bostock, M.G., 2000. Modelling teleseismic waves in dipping anisotropic structures. Geophys. J. Int. 141, 401-412.

A.2. Alsdorf, D., Makovsky, Y., Zhao, W., Brown, L.D., Nelson, K.D., Klemperer, S., Hauck, M., Ross, A., Cogan, M., Clark, M., Che, J., Kuo, J., 1998. INDEPTH (International Deep Profiling of Tibet and the Himalaya) multichannel seismic reflection data: Description and availability. J Geophys. Res. 103, 26993-26999.

A.3. Caldwell, W.B., Klemperer, S.L., Rai, S.S., Lawrence, J.F., 2009. Partial melt in the upper-middle crust of the northwest Himalaya revealed by Rayleigh wave dispersion. Tectonophysics 477, 58–65, doi:10.1016/j.tecto.2009.01.013.

A.4. Makovsky, Y., Klemperer, S. L., Ratschbacher, L., Alsdorf. D., 1999. Midcrustal reflector on INDEPTH wide-angle profiles: An ophiolite slab beneath the India-Asia suture in southern Tibet? Tectonics 18, 793–808.

A.5. Nábělek, J., György, H., Vergne, J., Sapkota, S., Kafle, B., Jiang, M., Su, H., Chen, J., Huang, B.S., Hi-CLIMB Team, 2009. Underplating in the Himalaya-Tibet collision zone revealed by the Hi-CLIMB experiment. Science 325, 1371-1374, doi: 10.1126/science.1167719.

A.6. Nábělek, P., Nábělek, J., 2014. Thermal characteristics of the Main Himalaya Thrust and the Indian lower crust with implications for crustal rheology and partial melting in the Himalaya orogen. Earth Planet. Sci. Lett., 395, 116–123.

A.7. Zhao, W., Kumar, P., Mechie, J., Kind, R., Meissner, R., Wu, Z., Shi, D., Su, H., Xue, G., Karplus, M. Tilmann, F., 2011. Tibetan plate overriding the Asian plate in central and northern Tibet. Nature Geoscience 4, 870-873.